

## The annealing mechanism of the radiation-induced vacancy-oxygen defect in silicon

V. V. Voronkov, R. Falster, and C. A. Londos

Citation: *J. Appl. Phys.* **111**, 113530 (2012); doi: 10.1063/1.4729323

View online: <http://dx.doi.org/10.1063/1.4729323>

View Table of Contents: <http://jap.aip.org/resource/1/JAPIAU/v111/i11>

Published by the [American Institute of Physics](#).

---

### Related Articles

Measurement of bonding energy in an anhydrous nitrogen atmosphere and its application to silicon direct bonding technology

*J. Appl. Phys.* **111**, 104907 (2012)

Optical transitions of InAs/GaAs quantum dot under annealing process

*J. Appl. Phys.* **111**, 104304 (2012)

Slip band distribution in rapid thermally annealed silicon wafers

*J. Appl. Phys.* **111**, 094901 (2012)

Shift of Ag diffusion profiles in CdTe by metal/semiconductor interfaces

*Appl. Phys. Lett.* **100**, 171915 (2012)

Evolution of electrical performance of ZnO-based thin-film transistors by low temperature annealing

*AIP Advances* **2**, 022118 (2012)

---

### Additional information on *J. Appl. Phys.*

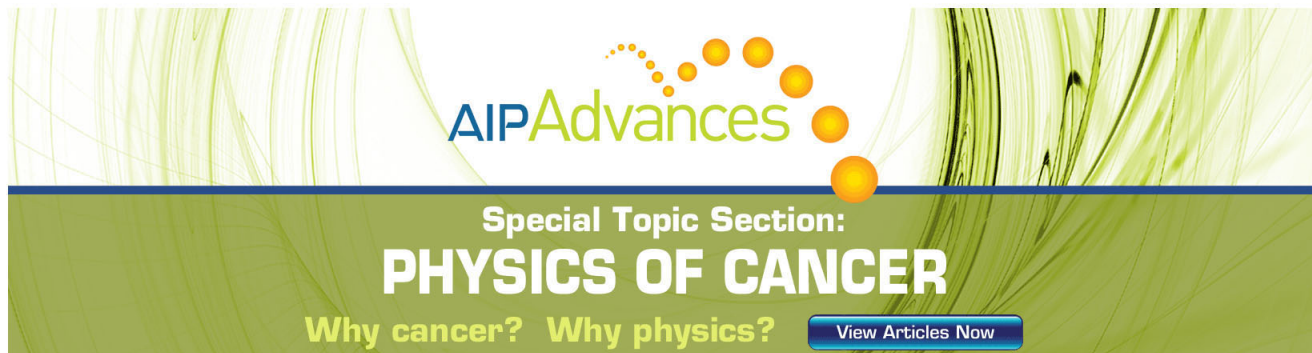
Journal Homepage: <http://jap.aip.org/>

Journal Information: [http://jap.aip.org/about/about\\_the\\_journal](http://jap.aip.org/about/about_the_journal)

Top downloads: [http://jap.aip.org/features/most\\_downloaded](http://jap.aip.org/features/most_downloaded)

Information for Authors: <http://jap.aip.org/authors>

## ADVERTISEMENT



**AIP Advances**

Special Topic Section:  
**PHYSICS OF CANCER**

Why cancer? Why physics? [View Articles Now](#)

## The annealing mechanism of the radiation-induced vacancy-oxygen defect in silicon

V. V. Voronkov,<sup>1,a)</sup> R. Falster,<sup>1</sup> and C. A. Londos<sup>2</sup>

<sup>1</sup>MEMC Electronic Materials, via Nazionale 59, Merano 39012, Italy

<sup>2</sup>University of Athens, Panepistiotopolis Zografos, Athens 15784, Greece

(Received 8 March 2012; accepted 11 May 2012; published online 14 June 2012)

Annealing experiments on the VO defect (the A-centre) produced by radiation in silicon—reported long ago—have been re-examined in order to deduce the two most important properties of VO: its diffusivity and the equilibrium constant for VO dissociation into V + O. The loss rate of VO is accounted for by two major reactions. One is the conventional reaction of the trapping of mobile VO by oxygen, thus producing VO<sub>2</sub>. The other is an annihilation of vacancies, which coexist in an equilibrium ratio with VO, by radiation-produced interstitial point defects. In some cases, a minor reaction, VO + V, should also be taken into account. The emerging minor defects V<sub>2</sub>O are also highly mobile. They partially dissociate back and partially get trapped by oxygen producing stable V<sub>2</sub>O<sub>2</sub> defects. © 2012 American Institute of Physics. [<http://dx.doi.org/10.1063/1.4729323>]

### I. INTRODUCTION

In electron-irradiated, lightly doped, high oxygen concentration silicon, vacancies produced by the radiation are mostly trapped by oxygen atoms.<sup>1-4</sup> The resulting VO defects, also called A-centres, give rise to an IR absorption band at 830 cm<sup>-1</sup> at  $T_{\text{room}}$ . Upon subsequent annealing at  $T > 300$  °C, this band disappears and a new band, 889 cm<sup>-1</sup>, emerges.<sup>2-4</sup> This latter band has been attributed to a VO<sub>2</sub> defect formed by a VO + O reaction that proceeds due to the relatively fast diffusion of VO, the diffusivity of monomeric interstitial oxygen O being too low in this temperature range.<sup>5</sup>

Vacancy trapping by oxygen into VO and VO<sub>2</sub> plays a crucial role also at high temperatures where it affects void formation during crystal growth<sup>6</sup> and vacancy-controlled oxygen precipitation.<sup>7</sup> Low- $T$  data on VO and VO<sub>2</sub> are indispensable to deduce the properties of these defects that can be then used to treat the above-mentioned high- $T$  phenomena.

For this purpose, data on isothermal annealing of VO are most useful. To our knowledge, such data were collected only long ago.<sup>2-4</sup> Other, subsequently published, data on isochronal annealing would require a separate, more complicated analysis. The final concentration of anneal-produced VO<sub>2</sub> is often smaller<sup>2-4</sup> than the initial concentration of VO and indicates some additional loss mechanism of VO apart from VO trapping by oxygen. In the present paper, it is shown that the reported kinetics of the isothermal loss of VO and of the rise of VO<sub>2</sub> can be well fitted by a combination of two basic reactions: 1) the above-mentioned VO trapping by oxygen and 2) the annihilation of VO through reversible dissociation into V + O with a subsequent annihilation of the released vacancies by radiation-induced self-interstitial defects. A refined value of VO diffusivity is obtained, and the equilibrium dissociation constant of VO is estimated.

These numbers provide an important link to high-temperature vacancy trapping by oxygen.

### II. FORMATION OF VO<sub>2</sub> AND THE DIFFUSIVITY OF VO

The time dependence of the 830 cm<sup>-1</sup> band intensity  $A_1$  (due to VO) and of the 889 cm<sup>-1</sup> band intensity  $A_2$  (presumably due to VO<sub>2</sub>) has been reported<sup>3</sup> for four temperatures in the range of 304 to 350 °C. An example is shown in Fig. 1. An increase in the concentration  $C_{V_2}$  of VO<sub>2</sub>—due to the VO + O reaction—is proportional to the concentration  $C_{V_1}$  of VO

$$dC_{V_2}/dt = \beta C_{V_1}. \quad (1)$$

The kinetic coefficient  $\beta$ , if diffusion-limited, is equal to

$$\beta = 4\pi r(D_{V_1} + D)C, \quad (2)$$

where  $C$  is the oxygen concentration,  $D_{V_1}$  and  $D$  are the diffusivities of VO and O, respectively. For the capture radius  $r$ , a conventional value of 0.5 nm is assumed. The VO band intensity  $A_1$  is equal to  $\gamma_1 C_{V_1}$ , where  $\gamma_1$  is the calibration coefficient. For the emerging VO<sub>2</sub>-related band at 889 cm<sup>-1</sup>, with intensity  $A_2$ , the calibration coefficient  $\gamma_2$  should be half as low as  $\gamma_1$  since this band is due to two weakly interacting oxygen atoms.<sup>3</sup> In other words,  $\gamma_2/\gamma_1 = 0.5$ , and Eq. (1) leads to an equation relating the two intensities

$$dA_2/dt = 2\beta A_1. \quad (3)$$

The  $A_1(t)$  function can be approximated by a smooth curve going as close as possible to the experimental points for  $A_1$ . The  $A_2(t)$  function is then calculated by Eq. (3). With a properly chosen (best-fit) value of  $\beta$ , this curve reproduces well the experimental points for  $A_2$  in Fig. 1. This is true also for all the other annealing temperatures. The temperature dependence of the best-fit values of  $\beta$  is shown in Fig. 2. A contribution of the interstitial oxygen diffusion into  $\beta$ —which is  $4\pi rDC$  by Eq. (2)—calculated with a known

<sup>a)</sup>Electronic mail: vvoronkov@memc.it.

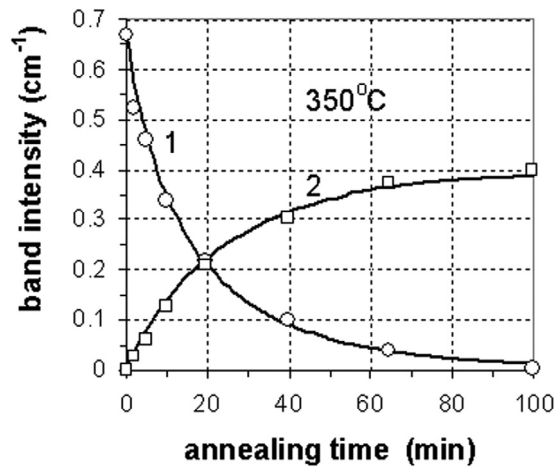


FIG. 1. IR intensities of the decaying VO defect (circles) and the emerging VO<sub>2</sub> defect (squares) in the course of annealing at 350 °C. The computed intensities are shown by solid curves.

oxygen diffusivity<sup>5</sup> is six orders of magnitude smaller than the actual value of  $\beta$ , in the temperature range of Fig. 2. Hence, the diffusivity sum in Eq. (2) is reduced to  $D_{V1}$ . The Arrhenius line drawn using all the four points corresponds to the activation energy of 2.1 eV. The prefactor of  $D_{V1}$  resulting from Eq. (2), with the reported oxygen concentration  $C = 7.9 \times 10^{17} \text{ cm}^{-3}$ , is enormously large, about  $60 \text{ cm}^2/\text{s}$ . On the other hand, the three higher- $T$  points in Fig. 2 reside on the straight line (solid curve in Fig. 2) of a slope 1.79 eV that corresponds to a reasonable prefactor of  $0.15 \text{ cm}^2/\text{s}$  and is almost the same as that for  $D$  (which is about  $0.13 \text{ cm}^2/\text{s}$ ). The last point in Fig. 2 may deviate from this line due to some inaccuracy in the reported nominal temperature of 304 °C (the actual  $T$  is probably somewhat lower). This explanation is supported by more arguments discussed below. The temperature dependence of  $D_{V1}$ —the diffusivity of VO—is now specified

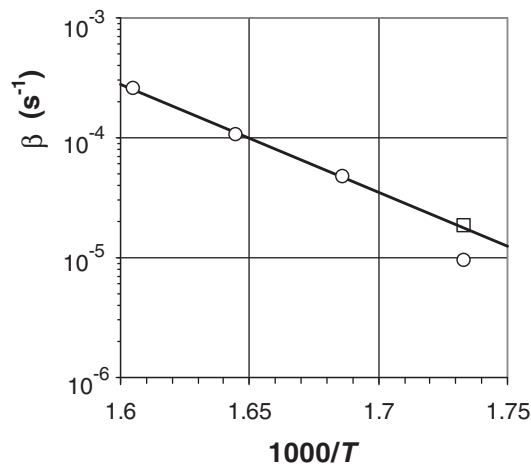


FIG. 2. The kinetic coefficient  $\beta$  for the VO + O reaction deduced from the kinetic curves of Ref. 3 (circles) available in a range of 304 to 350 °C, and of Ref. 2 (the square). The solid line is the adopted Arrhenius dependence.

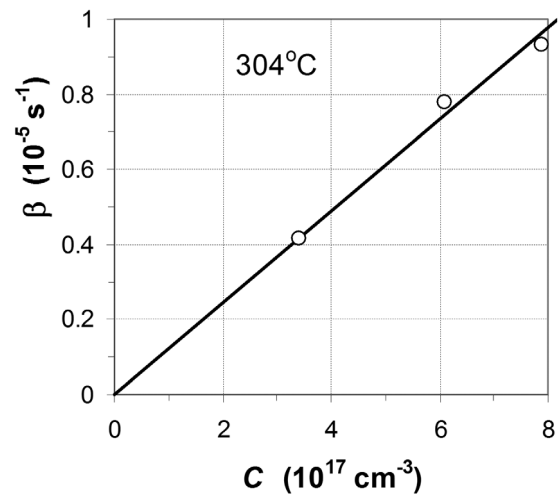


FIG. 3. The kinetic coefficient  $\beta$  for the VO + O reaction deduced from the kinetic curves<sup>3,4</sup> for samples of different oxygen content annealed at 304 °C.

$$D_{V1} = (0.15 \text{ cm}^2/\text{s}) \exp(-1.79 \text{ eV}/kT). \quad (4)$$

At 350 °C, this diffusivity is almost coincident with that used previously<sup>3</sup> in modelling the kinetic curves.

At the nominal temperature of 304 °C, there are two more reported kinetic curves<sup>4</sup> for samples of different oxygen concentrations. The deduced values of  $\beta$  in dependence of  $C$  are shown in Fig. 3. The expected proportionality of  $\beta$  to  $C$  is obeyed, strongly supporting the attribution of the emerging  $889 \text{ cm}^{-1}$  band to the VO<sub>2</sub> defect formed by VO + O reaction.

### III. THE LOSS OF VO

Mobile VO defects are trapped mostly by oxygen since other traps are of a far lower concentration. An additional loss mechanism of VO can be related to dissociation of VO into V + O. The vacancies released will be predominantly trapped back by oxygen for the same reason. Hence, an equilibrium ratio between the concentration  $C_V$  of released vacancies (V) and the concentration  $C_{V1}$  of trapped vacancies (VO) will be established

$$C_V C / C_{V1} = K_{V1}, \quad (5)$$

where  $K_{V1}$  is the equilibrium dissociation constant for VO. The fraction of V in the V + VO community (estimated below) is very small, but the vacancy diffusivity  $D_V$  is far larger than  $D_{V1}$ . The concentration of co-existing vacancy species,  $C_V + C_{V1} \approx C_{V1}$  will be reduced through vacancy trapping by radiation-induced interstitial defects and also by VO itself producing V<sub>2</sub>O.

To judge of the major loss path of the released vacancies it is helpful to look at the increment in the dissolved oxygen concentration,  $C(t)$ , measured<sup>3</sup> in the course of annealing at 335 °C. For sample #4—the same one for which the kinetic curves  $A_1(t)$ ,  $A_2(t)$  were reported—this increment is shown by circles in Fig. 4. The oxygen amount stored in the two observable defects VO and VO<sub>2</sub> can be thus calculated

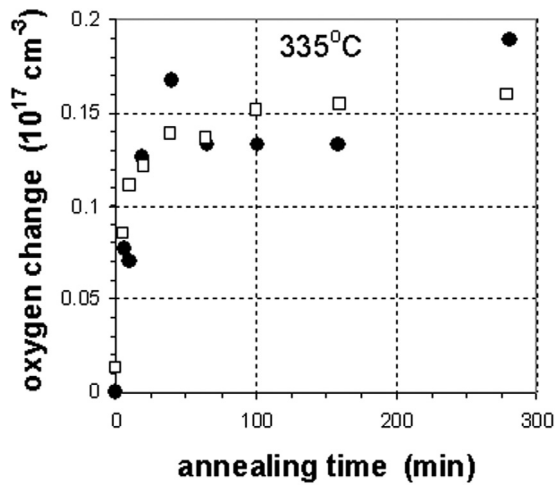


FIG. 4. Increment in the concentration of dissolved oxygen (circles) and decrement of oxygen concentration stored in VO and VO<sub>2</sub> defects (squares) in the course of annealing at 335 °C, by the data of Ref. 3.

$$C_{\text{stored}}(t) = C_{V1} + 2C_{V2} = \gamma_1(A_1 + A_2). \quad (6)$$

The decrement in the stored oxygen concentration, by Eq. (6), is presented in Fig. 4 by the squares using the calibration coefficient  $\gamma_1 = 6.25 \times 10^{16} \text{ cm}^{-2}$  determined in Ref. 8. This coefficient is coupled to the oxygen calibration  $\gamma = 2.4 \times 10^{17} \text{ cm}^{-2}$ , the same as that used in Ref. 3. The two quantities—the increment in the dissolved oxygen and the decrement in the stored oxygen—are almost coincident within the scatter of the data. This shows that there are no oxygen-containing species beside VO and VO<sub>2</sub> that emerge in an appreciable amount in the course of the anneal. The above-mentioned formation of V<sub>2</sub>O is thus concluded to be insignificant, either due to a too slow V + VO reaction, or due to a fast backward dissociation of V<sub>2</sub>O that prevents accumulation of V<sub>2</sub>O in an appreciable concentration.

The dominant defects that trap vacancies are hence considered to be radiation-induced interstitial defects. In lightly doped material, radiation-produced self-interstitials (I) are trapped mostly by the substitutional carbon atoms C<sub>s</sub>, and the resulting interstitial carbon atoms C<sub>i</sub> are quickly trapped by oxygen.<sup>9</sup> The major interstitial species is then C<sub>i</sub>O. This is true if the initial (prior to irradiation) carbon concentration is higher than the produced concentration of VO but lower than the oxygen concentration (otherwise there would be two interstitial species, C<sub>i</sub>O and C<sub>i</sub>C<sub>s</sub>, in comparable concentrations<sup>10</sup>). An anneal-induced loss of VO is accompanied by a conversion of C<sub>i</sub>O into C<sub>s</sub>O due to the trapping reaction V + C<sub>i</sub>O. Both these carbon species are optically active and can be monitored by their known IR bands. The expected loss of C<sub>i</sub>O and increase of C<sub>s</sub>O were indeed found.<sup>11</sup>

The concentration  $N_i$  of interstitial C<sub>i</sub>O defects is equal to the total concentration  $C_{V1} + C_{V2}$  of the vacancy species since V and I were produced by radiation in equal amounts. The loss rate of VO due to vacancy trapping is proportional to  $C_V N_i$ . The proportionality coefficient is  $4\pi r D_V$  for diffusion-limited reaction. Since  $C_V$  is proportional to  $C_{V1}$  by Eq. (5), the total loss rate of VO (including trapping of mobile VO by oxygen) is equal to

$$dC_{V1}/dt = -\alpha C_{V1}(C_{V1} + C_{V2}) - \beta C_{V1}. \quad (7)$$

The kinetic coefficient  $\alpha$ , for diffusion-limited trapping of vacancies by C<sub>i</sub>O, is

$$\alpha = 4\pi r D_V K_{V1}/C. \quad (8)$$

Note that the two kinetic coefficients in Eq. (7) are of an opposite dependence on the oxygen concentration:  $\beta$  is proportional to  $C$  while  $\alpha$  is inversely proportional to  $C$  because the concentration of released vacancies is inversely proportional to  $C$  by Eq. (5). For low oxygen content, the VO + O reaction will be much slower than the vacancy annihilation, and  $C_{V2}$  will be small in comparison to  $C_{V1}$  (at least for not too long annealing). In this case, the loss of VO is approximately a second-order reaction—with a rate proportional to  $C_{V1}^2$ . There is only one example of reported VO annealing kinetics corresponding to a low  $C$  and at the same time to a relatively high carbon content (to justify the present model, Eq. (7)). This is sample #8 of Ref. 4. As expected, the intensity  $A_2$  is extremely small for this sample. For the second-order kinetics,  $1/C_{V1}$  (and hence  $1/A_1$ ) is a linear function of the annealing time and this is indeed the case for this sample (Fig. 5).

At low carbon concentration—around  $10^{16} \text{ cm}^{-3}$ —the radiation-induced interstitial defects are represented by several species: C<sub>i</sub>O, IC<sub>i</sub>O, I<sub>2</sub>C<sub>i</sub>O, I<sub>3</sub>C<sub>i</sub>O, etc. co-existing in comparable concentrations.<sup>12</sup> One would expect the vacancy annihilation to be a complicated process accompanied by a change in the relative concentrations in the trap population. In spite of this, Eq. (7)—if formally applied to low-carbon samples—provides a surprisingly good fit, with a proper choice of the coefficient  $\alpha \gamma_1$  that enters Eq. (7) after the concentrations are expressed through the intensities  $A_1$  and  $A_2$ . The other coefficient,  $\beta$ , was already fitted as described above. The time dependence of  $A_1$  and  $A_2$ —obtained by integration of Eqs. (7), (1)—is shown by solid curves in Fig. 1; the computed  $A_2(t)$  curve is almost indistinguishable from that calculated before. Similarly, good fits were obtained for

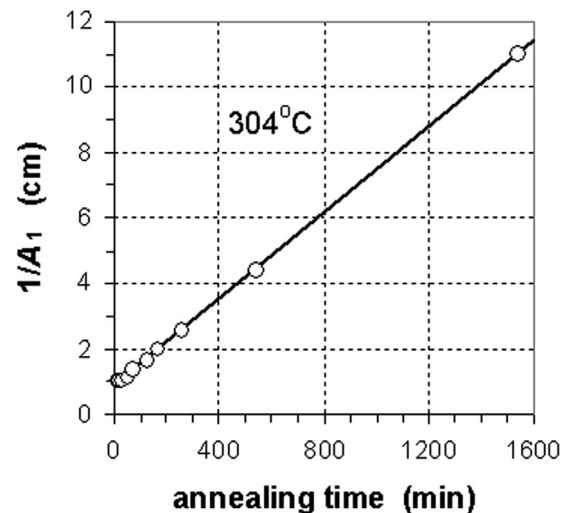


FIG. 5. Reciprocal IR intensity of VO in dependence of the annealing time at 304 °C, for the sample of a low oxygen content, after Ref. 4.

all the other annealing temperatures. A possible explanation of such a good fit is that the vacancy capture radius  $r$  by an  $I_nC_iO$  defect is proportional to the number of self-interstitials stored in this defect,  $n + 1$ . The overall trapping rate—a sum over all  $I_nC_iO$  defects—will be then proportional to the total concentration of stored self-interstitials, which is identical to  $C_{V1} + C_{V2}$ .

The deduced best-fit values of  $\alpha \gamma_1$  are plotted in dependence of  $\beta$  in Fig. 6. If both parameters strictly follow Arrhenius-type temperature dependence, with activation energies  $E_a$  for  $\alpha$  and  $E_b$  for  $\beta$ , then the dependence of  $\alpha$  on  $\beta$  should be of a power-law type, with an exponent  $E_a/E_b$ . In other words, a double-logarithmic plot should be linear, with a slope equal to  $E_a/E_b$ . An advantage of such a representation is that it is independent of the reported temperatures of annealing, whether these temperatures are accurate or not. For all the 4 samples represented in Fig. 6, the linearity is well obeyed, and the deduced energy ratio is  $E_a/E_b = 1.22$ . Hence,  $E_a = 2.2$  eV. The kinetic coefficient  $\alpha(T)$  is thus defined. The combination  $D_V K_{V1}$  that enters Eq. (8) for  $\alpha$  is then specified (using the reported oxygen concentration  $C = 7.9 \times 10^{17} \text{ cm}^{-3}$ ):

$$D_V K_{V1} = (2 \times 10^{22} \text{ cm}^{-1} \text{ s}^{-1}) \exp(-2.2 \text{ eV}/kT). \quad (9)$$

The vacancy diffusivity for a material of intrinsic conductivity—when the vacancy is most likely in the neutral charge state—was reported<sup>13</sup> to be

$$D_V = (0.0012 \text{ cm}^2/\text{s}) \exp(-0.45 \text{ eV}/kT). \quad (10)$$

The equilibrium dissociation constant  $K_{V1}$  of VO is then defined by Eqs. (9) and (10)

$$K_{V1} = (1.7 \times 10^{25} \text{ cm}^{-3}) \exp(-1.75 \text{ eV}). \quad (11)$$

A ratio of free to bound vacancies in the V + VO community is equal to  $K_{V1}/C$  by Eq. (5); at  $T < 350$  °C, it is very small—less than  $10^{-7}$ . This ratio however increases quickly upon

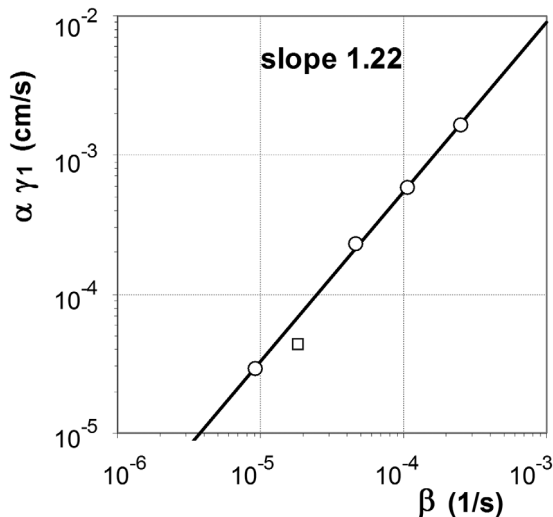


FIG. 6. The deduced kinetic coefficient  $\alpha \gamma_1$  (for VO loss due to vacancy annihilation) plotted in dependence of the deduced kinetic coefficient  $\beta$  (for VO loss due to trapping by oxygen). The circles are by the data of Ref. 3 (the oxygen concentration is  $7.9 \times 10^{17} \text{ cm}^{-3}$ ). The square is by the data of Ref. 2 (the oxygen concentration is probably a bit higher).

raising  $T$  and becomes 1 at  $T = 930$  °C for a representative oxygen concentration of  $8 \times 10^{17} \text{ cm}^{-3}$ . This “temperature of vacancy binding by oxygen” can be considered as a rough estimate since  $K_{V1}$  was extrapolated through 7 orders of magnitude. Another rough estimate for the binding temperature—around 1050 °C—was obtained<sup>6</sup> from the data on void formation during crystal growth; the activation energy for  $K_{V1}$  was estimated as 1.85 eV. These earlier estimates are not very far from the presently obtained ones. A link between low- $T$  and high- $T$  data on vacancy trapping by oxygen is thus established.

#### IV. THE SATURATED CONCENTRATION OF VO<sub>2</sub>

Upon combining Eqs. (1) and (7), an equation relating  $C_{V1} + C_{V2}$  and  $C_{V2}$  is obtained

$$d(C_{V1} + C_{V2})/dC_{V2} = -(\alpha/\beta)(C_{V1} + C_{V2}). \quad (12)$$

Initially,  $C_{V1} = C_{V10}$  and  $C_{V2} = 0$ . Upon increasing the annealing time  $C_{V1}$  decreases down to 0 while  $C_{V2}$  increases up to a saturated (final) value  $C_{V2f}$ . The integration of Eq. (12) results in a relation between  $C_{V10}$  and  $C_{V2f}$

$$C_{V2f} = (\beta/\alpha) \log(C_{V10}/C_{V2f}). \quad (13)$$

In terms of the corresponding intensities  $A_{10}$  and  $A_{2f}$ , this relation reads

$$A_{2f} = [2\beta/(\alpha\gamma_1)] \log(2A_{10}/A_{2f}). \quad (14)$$

Since the ratio  $\beta/\alpha$  is proportional to the squared oxygen concentration, it is convenient to normalize each intensity by dividing it by  $(C/C_0)^2$ , where  $C_0$  is some reference oxygen concentration (adopted here to be  $10^{18} \text{ cm}^{-3}$ ). Thus, the relation (14) contains only one parameter,  $\beta_0/(\alpha_0\gamma_1)$ , where the kinetic coefficients marked by the subscript 0 are taken at  $C = C_0$ . The computed dependence of the  $A_{2f}/A_{10}$  ratio on the normalized starting intensity of VO (with  $\beta_0/(\alpha_0\gamma_1) = 0.37 \text{ cm}^{-1}$ ) is shown in Fig. 7 together with the experimental data<sup>4</sup> for samples of

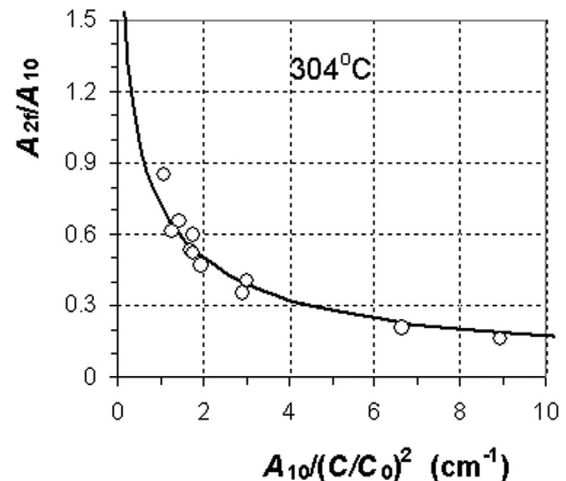


FIG. 7. The ratio of the saturated IR intensity  $A_{2f}$  (of VO<sub>2</sub>) and the initial IR intensity  $A_{10}$  (of VO) plotted in dependence of  $A_{10}/(C/C_0)^2$  where  $C$  is the actual oxygen concentration and  $C_0 = 10^{18} \text{ cm}^{-3}$  is a reference oxygen concentration. The solid line is the predicted dependence by Eq. (14).

different oxygen content and of different starting intensity  $A_{10}$ . Strictly speaking, Eq. (12) and the resulting relation (14) are only well justified for carbon-rich samples, and yet the computed curve in Fig. 7 gives a good fit to the data for all the samples most of which are carbon-lean.

## V. A POSSIBLE INVOLVEMENT OF $V_2O$ AND $V_2O_2$ DEFECTS

The evolution of the  $830\text{ cm}^{-1}$  band reported by Corbett *et al.*<sup>2</sup> was different from that analyzed above by one minor but remarkable feature: the intensity  $A_1$  did not tend to zero upon prolonged isothermal annealing at  $304\text{ }^\circ\text{C}$ . Furthermore, isochronal annealing also showed<sup>2</sup> that the intensity  $A_1$ —after an initial reduction—stayed constant up to  $400\text{ }^\circ\text{C}$ . VO defects cannot survive in this temperature range: the loss time of VO due to only  $\text{VO} + \text{O}$  reaction (which is  $1/\beta$ ) becomes 5 min at  $400\text{ }^\circ\text{C}$ . This means that the residual  $830\text{ cm}^{-1}$  band is not due to VO but rather to the  $V_2O_2$  defect that is expected<sup>3</sup> to have the same band as VO. These  $V_2O_2$  defects may originate from the mobile  $V_2O$  species that are trapped by oxygen.  $V_2O$  defects, as mentioned above, can be produced by the trapping reaction  $\text{VO} + \text{V}$  (and also by trapping the radiation-produced divacancy by oxygen). Since the  $V_2O$  defect<sup>14</sup> has an IR band at  $826\text{ cm}^{-1}$ —well distinguished from that of VO—it cannot account for the residual  $830\text{ cm}^{-1}$  band. The identification of the residual band with  $V_2O_2$  is supported by the fact that at  $T > 400\text{ }^\circ\text{C}$  this band starts to disappear accompanied by a rise in the  $\text{VO}_2$ -related band,  $889\text{ cm}^{-1}$ . Apparently, self-interstitials start to be released by the remaining (not yet annihilated) interstitial point defects at these temperatures and  $V_2O_2$  is converted into  $\text{VO}_2$  by the  $V_2O_2 + \text{I}$  reaction.

Why is the same reaction sequence,  $\text{VO} + \text{V}$  and  $V_2O + \text{O}$ —which leads to a small but detectable amount of  $V_2O_2$ —not manifested in the kinetic curves discussed above? A difference may be in the population of the interstitial defects. In case of Corbett *et al.*,<sup>2</sup> a release of I by these defects does not occur until the relatively high temperature of  $400\text{ }^\circ\text{C}$ . In other cases, such a release may start at lower  $T$ .  $V_2O$  defects are then converted back into VO by  $V_2O + \text{I}$  reaction thus preventing their conversion into  $V_2O_2$ .

To simulate the case of Corbett *et al.*, two additional reactions should be included into the model. The concentration of  $V_2O$ —denoted  $C^*$ —is changed by two reactions. The first one is the formation of this species by the forward reaction  $\text{V} + \text{VO}$  accompanied by a loss due to the backward dissociation of  $V_2O$

$$dC^*/dt = \alpha^*(C_{V1}^2 - \chi C^*C), \quad (15)$$

where the forward kinetic coefficient  $\alpha^*$ —if diffusion—limited—is similar to  $\alpha$  as defined by Eq. (8), and  $\chi$  is the equilibrium constant. The reaction (15) leads to a change in  $C_{V1}$  while the sum  $C_{V1} + 2C^*$  (the total amount of stored vacancies) stays unchanged. The dissociation time  $\tau^*$  of  $V_2O$  is expressed from Eq. (15) as  $1/(\alpha^*\chi C)$ . This dissociation time was reported<sup>15</sup> in a range of  $280$  to  $350\text{ }^\circ\text{C}$ . It is

about  $350$  min at  $304\text{ }^\circ\text{C}$ . With a specified  $\tau^*$ , there is only one fitting parameter in reaction (15): either  $\alpha^*$  or  $\chi$ .

The other reaction is the irreversible trapping of mobile  $V_2O$  by oxygen

$$dC^*/dt = -\beta^*C^*, \quad (16)$$

which leads to an increase in the  $V_2O_2$  concentration. The kinetic coefficient  $\beta^*$  is expressed through the diffusivity  $D^*$  of  $V_2O$  similar to Eq. (2).

The computed intensity  $A_1(t)$  is now the combination of the two contributions: of VO and of  $V_2O_2$ . The calibration coefficient for the latter defect is half that for VO due to the two equivalent oxygen atoms in  $V_2O_2$ . The previous model—based only on reactions (1) and (7)—cannot reproduce the observed<sup>2</sup> kinetic curves  $A_1(t)$  and  $A_2(t)$ . However, the modified model—including reactions (15) and (16)—gives a good fit with  $\chi \approx 0.3$  and  $\beta^* \approx 10^{-4}\text{ s}^{-1}$  (Fig. 8). The best-fit values of  $\alpha$  and  $\beta$  (insensitive to the assumed  $\chi$ ) are represented by the square in Fig. 6. The oxygen concentration was not specified,<sup>2</sup> but it is unlikely to deviate much from the value of  $7.9 \times 10^{17}\text{ cm}^{-3}$  for the other data points (circles). A position of the new point is slightly below the straight line, indicating a slightly higher value of  $C$  for this sample (leading to a smaller  $\alpha$  and a higher  $\beta$ ). The kinetic coefficient  $\beta$  is shown also in Fig. 2, again by the square. This point resides rather close to the straight line in this figure suggesting that the reported<sup>2</sup> nominal temperature of  $304\text{ }^\circ\text{C}$  is closer to the actual temperature than in case of Refs. 3 and 4.

The computed intensities of  $V_2O$  (with a calibration coefficient identical to  $\gamma_1$ ) and of  $V_2O_2$  (with a calibration coefficient  $\gamma_1/2$ ) are also shown in Fig. 8 for the sake of illustration. The  $V_2O$  defect is formed only at an early stage of annealing. Later it disappears due to both dissociation and due to trapping by oxygen into  $V_2O_2$ . For the best-fit parameters,  $\alpha^*/\alpha = 0.3$  and  $\beta^*/\beta = 5.6$ . The latter number shows that the diffusivity of  $V_2O$  defect is somewhat higher than that of VO.

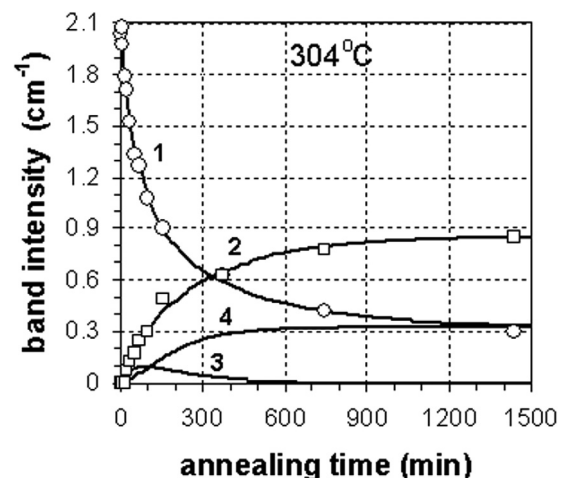


FIG. 8. The measured IR intensities<sup>2</sup> of  $830\text{ cm}^{-1}$  band (due to VO and  $V_2O_2$ ) and of  $889\text{ cm}^{-1}$  band (due to  $\text{VO}_2$ ) in the course of annealing at  $304\text{ }^\circ\text{C}$  (circles and squares, respectively). The solid curves 1 and 2 drawn through these points have been simulated. The curve 3 shows the computed IR intensity due to  $V_2O$  and the curve 4 due to  $V_2O_2$ .

## VI. SUMMARY

Data on isothermal annealing of radiation-induced VO defects—reported long-ago—were re-examined to deduce more information on the parameters of relevant reactions.

First, the diffusivity of VO was accurately determined in dependence of temperature; the migration energy was concluded to be 1.79 eV while the prefactor is almost coincident with that for monomeric interstitial oxygen.

Second, the loss of VO was shown to correspond well to two major reaction paths:

- 1) Trapping of mobile VO species by oxygen—with a rate proportional to the oxygen concentration  $C$ .
- 2) Trapping of vacancies—released by VO—by radiation-induced interstitial defects. The released vacancies are mostly trapped back by oxygen and therefore exist in equilibrium with VO, in a low concentration inversely proportional to  $C$ . Accordingly, the loss rate of VO by this path is also inversely proportional to  $C$ .

At low  $C$ , the loss of VO occurs mostly by the second path and corresponds to a second-order reaction of annihilation of the interstitial defects by VO (through released vacancies).

By the deduced reaction constant for the second loss path, the equilibrium dissociation constant of VO was determined; the binding energy of V to O was found to be

1.75 eV. It is close to a previous estimate of 1.85 eV based on high- $T$  data.<sup>6</sup>

Along with the above-mentioned two major reactions, there is also vacancy trapping by VO that produces  $V_2O$  defects (in a relatively low concentration). These species exist only temporarily being partially dissociated and partially trapped by oxygen into a  $V_2O_2$  defect that gives rise to the same IR band as VO.

<sup>1</sup>G. D. Watkins, *J. Phys. Soc. Jpn.* **18** (Suppl. II), 22 (1963).

<sup>2</sup>J. W. Corbett, G. D. Watkins, and R. S. McDonald, *Phys. Rev.* **135**, A1381 (1964).

<sup>3</sup>B. G. Swensson and J. L. Lindstrom, *Phys. Rev. B* **34**, 8709 (1986).

<sup>4</sup>J. L. Lindstrom, G. S. Oehrlein, and J. W. Corbett, *Phys. Status Solidi A* **95**, 179 (1986).

<sup>5</sup>J. Mikkelsen, *Mater. Res. Soc. Symp. Proc.* **59**, 19 (1986).

<sup>6</sup>V. V. Voronkov and R. Falster, *J. Electrochem. Soc.* **149**, G167 (2002).

<sup>7</sup>V. V. Voronkov and R. Falster, *J. Appl. Phys.* **91**, 5802 (2002).

<sup>8</sup>A. S. Oates and R. C. Newman, *Appl. Phys. Lett.* **49**, 262 (1986).

<sup>9</sup>G. Davies, E. C. Lightowers, R. C. Newman, and A. S. Oates, *Semicond. Sci. Technol.* **2**, 524 (1987).

<sup>10</sup>G. Davies, Kwok Tat Kun, and T. Reade, *Phys. Rev. B* **44**, 12146 (1991).

<sup>11</sup>A. Chroneos, C. A. Londos, and E. N. Sgourou, *J. Appl. Phys.* **110**, 093507 (2011).

<sup>12</sup>V. V. Voronkov, R. Falster, C. A. Londos, E. N. Sgourou, A. Andrianakis, and H. Ohyama, *J. Appl. Phys.* **110**, 093510 (2011).

<sup>13</sup>G. D. Watkins, *J. Appl. Phys.* **103**, 106106 (2008).

<sup>14</sup>L. I. Murin, B. G. Swensson, J. L. Lindstrom, V. P. Markevich, and C. A. Londos, *Solid State Phenom.* **156–158**, 129 (2010).

<sup>15</sup>M. Mikelsen, J. H. Bleka, J. S. Christensen, E. V. Monakhov, B. G. Swensson, J. Harkonen, and B. S. Avset, *Phys. Rev. B* **75**, 155202 (2007).